3-1-1999

A Note on Gravity Wave-driven Volume Emission Rate Weighted Temperature Perturbations Inferred from O_2 Atmospheric and O I 5577 Airglow Observations

Michael P. Hickey Ph.D.
Embry-Riddle Aeronautical University, hicke0b5@erau.edu

Richard L. Walterscheid
The Aerospace Corporation

Scholarly Commons Citation

Hickey, M. P., and R. L. Walterscheid (1999), A note on gravity wave-driven volume emission rate weighted temperature perturbations inferred from O2 atmospheric and O I 5577 airglow observations, J. Geophys. Res., 104(A3), 4279–4286, doi: https://doi.org/10.1029/1998JA900164

JOURNAL OF GEOPHYSICAL RESEARCH, VOL. 104, NO. A3, PAGES 4279–4286, MARCH 1, 1999

A note on gravity wave-driven volume emission rate weighted temperature perturbations inferred from O_2 atmospheric and O I 5577 airglow observations

Michael P. Hickey

Department of Physics and Astronomy, Clemson University, Clemson, South Carolina

Richard L. Walterscheid

Space and Environment Technology Center, The Aerospace Corporation, Los Angeles, California

Abstract. A full-wave dynamical model and chemistry models that simulate ground-based observations of gravity wave-driven O_2 atmospheric and O I 5577 airglow fluctuations in the mesopause region are used to demonstrate that for many observable gravity waves modeling is required to infer temperature perturbation amplitudes from airglow observations. We demonstrate that the amplitude of the altitude-integrated volume emission rate weighted temperature perturbation differs by at least about 30% from the amplitude of the temperature perturbation of the major gas in the vicinity of the peak of the airglow volume emission rate for gravity waves with horizontal phase speeds less than about 150 m s^{-1} and vertical wavelengths less than about 50 km and that the amplitude of the altitude-integrated volume emission rate weighted temperature perturbation differs considerably from the amplitude of the temperature perturbation averaged over the vertical extent of the emission layer for waves with horizontal phase speeds less than about 65 m s^{-1} and vertical wavelengths less than about 20 km. For waves with phase speeds less than about 100 m s^{-1} and vertical wavelengths less than about 30 km the amplitude of the altitude-integrated volume emission rate weighted temperature perturbation differs by at least about 30% from the altitude-integrated mean volume emission rate weighted temperature perturbation, demonstrating that the nonthermal fluctuation contribution to the former (involving volume emission rate perturbations) needs to be included in such modeling. We conjecture that the observed brightness perturbation is a simpler and better quantity to simulate using detailed modeling than the observed airglow temperature perturbation for the determination of wave amplitude in cases where nonthermal effects or cancellation effects (for short vertical wavelengths) are strong.

1. Introduction

Airglow observations can provide useful information about gravity waves in the mesopause region. Airglow emissions such as the OH Meinel and the O_2 atmospheric can provide a measure of temperature in addition to airglow brightness, and numerous studies based on both observation and theory have related the measured airglow brightness fluctuations to the measured fluctuations in the derived temperature [see *Hickey et al.*, 1993, 1997, and references therein]. Additionally, one study has related long period brightness fluctuations to temperature fluctuations using the O I 5577 emission (G. Schubert et al., Theory and observations of gravity wave induced fluctuations in the O I (557.7 nm) airglow, submitted to *Journal of Geophysical Research*, 1998, hereinafter referred to as submitted manuscript, 1998). One significant drawback of the airglow measurements is that usually wave amplitude cannot be directly inferred from such measurements, although a combination of modeling and measurement of the airglow brightness fluctuations can provide some constraint on wave amplitude, as discussed by *Hickey et al.* [1997, 1998] and *Swenson and Gardner* [1998].

In some studies it has been assumed that the measured airglow temperature fluctuations can provide a reasonable estimate of either the gravity wave temperature fluctuation amplitude in the vicinity of the peak of the airglow volume emission rate or the mean temperature perturbation averaged over the vertical extent of the emission layer [e.g., *Hecht and Walterscheid*, 1991]. However, neither of these assumptions have been validated. In this paper these assumptions are investigated using a dynamical full-wave model coupled with chemistry models describing the effects of gravity waves on airglow emissions. Specifically, we model the volume emission rate weighted temperature fluctuation $\langle T_I' \rangle$ [e.g., *Schubert and Walterscheid*, 1988; *Swenson and Gardner*, 1998] and compare it directly to both the gravity wave temperature fluctuation at the emission peak, $T'_{at-peak}$, and the gravity wave temperature fluctuation averaged over the vertical extent of the emission layer, T'_{avg} (for the latter this vertical extent is defined by the altitudes where the mean, undisturbed volume emission rate has fallen to one-tenth of its peak value, which corresponds to approximately 15 km). Our primary objective is to determine the value of phase speed and

Paper number 1998JA900164.
0148-0227/99/1998JA900164$09.00

vertical wavelength at which $\langle T_I' \rangle$ begins to differ from both $T'_{at-peak}$ and T'_{avg}. These differences are primarily due to the effects of interference (cancellation), which are more important for the shorter vertical wavelength waves. $\langle T_I' \rangle$ includes both thermal and nonthermal contributions. The thermal contribution equals the altitude-integrated temperature perturbation weighted by the mean volume emission rate ($\langle T_I' \rangle$) and is the only contributor in an isothermal atmosphere. The nonthermal contributions are due to perturbations in the volume emission rate. Another objective of this study is to compare $\langle T_I' \rangle$ to $\langle T_I' \rangle$ in order to determine for which waves the nonthermal contribution to $\langle T_I' \rangle$ becomes important. We will demonstrate that for many observable gravity waves $\langle T_I' \rangle$ differs considerably from $T'_{at-peak}$, T'_{avg}, and $\langle T_I' \rangle$, which suggests that modeling including the nonthermal fluctuation contribution (involving volume emission rate fluctuations, I') is required to determine the true gravity wave amplitude.

We also distinguish between two different interference effects in these quantities. The first is associated with the finite thickness of the emission layer and occurs in the limit of short vertical wavelength (λ_z) where cancellation along the line of sight becomes severe. The second is associated with waves of large λ_z (including evanescent waves) for which inhomogeneities in the mean temperature profile lead to wave reflection. In extreme cases wave reflection leads to ducting. The airglow response to ducted waves has been studied by *Hines and Tarasick* [1994] and *Makhlouf et al.* [1998] with respect to the so-called Krassovsky's ratio. However, the volume emission rate weighted temperature perturbation associated with wave reflection has not been explicitly discussed before.

The airglow emissions that we model here are the O_2 atmospheric 0-1 band (that derives from a two-step process in which the intermediate state, which we assume to be $O_2(c^1\Sigma_u^-)$, is quenched by O_2 to form $O_2(b^1\Sigma_g^+)$, which subsequently decays to the $O_2(X^3\Sigma_g^-)$ state) and the O I 5577 (that derives from the same two-step process in which the intermediate state $O_2(c^1\Sigma_u^-)$ is quenched by O to form $O(^1S)$, which subsequently decays to $O(^1D)$). Both of these emissions are produced by an initial three-body recombination reaction of atomic oxygen, and so there are similarities in the chemical schemes describing them. The chemical schemes that we employ have been described by *Hickey et al.* [1993, 1998]. We model the steady state response of the minor species $O_2(b^1\Sigma_g^+)$ and $O(^1S)$ (and concomitant O_2 atmospheric and O I 5577 airglow emissions) to gravity wave forcing. This requires that we employ a full-wave model to define the waves in a nonisothermal atmosphere. We compare $\langle T_I' \rangle$ to each of $\langle T_I' \rangle$, $T'_{at-peak}$, and T'_{avg} for each emission and for a wide range of wave parameters (horizontal phase speed and horizontal wavelength).

The layout of this paper is as follows. In section 2 we discuss the theory of volume emission rate weighted temperature fluctuations in the nightglow, while in section 3 we discuss the model used to simulate these fluctuations in the O_2 atmospheric and O I 5577 nightglows. The results are presented in section 4, and a discussion of these results is given in section 5. Finally, our conclusions are presented in section 6.

2. Theory

The volume emission rate weighted temperature perturbation ($\langle T_I' \rangle$) derived from airglow observations has been discussed by *Schubert and Walterscheid* [1988] and is defined as

$$\langle T_I \rangle = \langle IT \rangle / \langle I \rangle \tag{1}$$

where the angled brackets denote integration of the enclosed

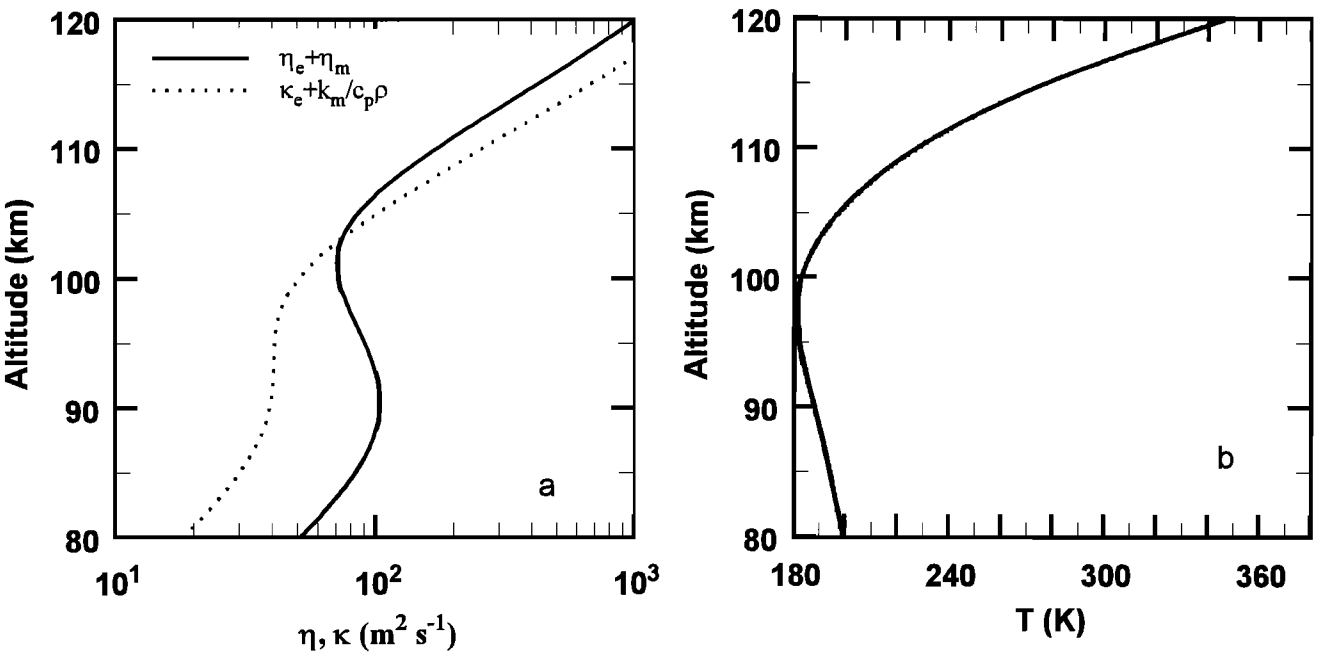

Figure 1. (a) Altitude profile of the molecular plus eddy momentum (solid curve) and thermal (dotted curve) diffusivities employed in the full-wave model (b) Mean temperatures derived from the MSIS-90 model employed in the computations

variable over the vertical extent of the airglow emission, and where I is airglow volume emission rate and T is atmospheric temperature. (Note that the altitude-integrated volume emission rate, $\langle I \rangle$, is the brightness.) We let both the airglow volume emission rate and temperature comprise a mean (bearing an overbar) and a perturbation about that mean (primed) and expand (1) to first order so that the volume emission rate weighted temperature perturbation ($\langle T_I' \rangle$) is given by

$$\langle T_I' \rangle = \langle T_I' \rangle + \frac{\langle \bar{T} I' \rangle}{\langle \bar{I} \rangle} - \frac{\langle \bar{T} \bar{I} \rangle \langle I' \rangle}{\langle \bar{I} \rangle^2} \quad (2)$$

where $\langle T_I' \rangle$ is the altitude-integrated temperature perturbation weighted by the mean volume emission rate ($\bar{I}$):

$$\langle T_I' \rangle = \langle \bar{I} T' \rangle / \langle \bar{I} \rangle \quad (3)$$

Equation (2) shows that for an isothermal atmosphere the two nonthermal terms cancel and $\langle T_I' \rangle$ is exactly equal to $\langle T_I' \rangle$. Thus volume emission rate fluctuations (I') do not explicitly contribute to $\langle T_I' \rangle$ in an isothermal atmosphere. For a nonisothermal atmosphere, (2) shows that volume emission rate fluctuations explicitly contribute to $\langle T_I' \rangle$ meaning that there can be apparent fluctuations in the volume emission rate weighted temperature even when T' is zero.

In both (2) and (3) the integrals of terms involving fluctuations can be very small for waves with vertical wavelengths less than the emission layer thickness due to the effects of destructive interference. Additionally, the relative contribution of individual fluctuations to the altitude integrals in (2) and (3) will also depend on the altitude variation of wave amplitude, and so we expect that the integrals may also depend on the effects of dissipation.

3. Model

The full-wave model used in these computations has been described by *Hickey et al.* [1997, 1998] and G. Schubert et al. [submitted manuscript, 1998]. The linear, steady state model simulates gravity wave propagation in an inhomogeneous atmosphere. Wave dissipation is due to the effects of the eddy diffusion of heat and momentum in the middle atmosphere and molecular and ion-drag dissipation in the thermosphere. The model also includes the effects of the Coriolis force. The full-wave model produces the perturbation velocities (the two horizontal components and the vertical component), and the perturbation temperature and pressure, all output as a function of altitude. These perturbations are then input to a steady-state model describing O(^1S) emission fluctuations, as described by *Hickey et al.* [1997, 1998], and also for the O_2 atmospheric emission using the chemistry described by *Hickey et al.* [1993]. For all of the results presented here the Gaussian source in the full-wave model was located at an altitude of 60 km with a full-width half-maximum of 0.125 km. The lower boundary was the ground, and the upper boundary was located somewhere between 200 and 500 km, the greater altitudes corresponding to the faster waves, as discussed by *Hickey et al.* [1997, 1998]. A total number of 38,000 points were used on the altitude grid, corresponding to a vertical resolution that varied from about 5.3 to 13 m for the slower and faster waves, respectively

The eddy diffusion profile used in the full-wave model computations is shown in Figure 1a and maximizes at 90 km with a value of 100 m^2 s^{-1}. The Prandtl number relating the momentum and thermal diffusivities is 3. The mean temperature profile used in the computations is shown in Figure 1b and was derived from the MSIS-90 model for 18°N near local midnight on April 9. The $F_{10.7}$ and a_p inputs were 87 and 12, respectively. The mesopause is moderately high (about 97.5 km), and temperature gradients are about -0.8 K km^{-1} between about 90 and 97 km, and exceed 1 K km^{-1} above about 100 km. The O number density profile derived from the MSIS-90 model and the corresponding O_2 atmospheric and O I 5577 airglow volume emission rate profiles (using the airglow chemistry parameters presented by *Hickey et al.* [1993, 1998]) are shown in Figure 2. The important features of this figure are that the O_2 atmospheric volume emission rate peaks near 93 km altitude (about 4.5 km below the mesopause), while the O I 5577 volume emission rate peaks near 95.5 km altitude (about 2 km below the mesopause, according to the MSIS-90 model for the described inputs).

4. Results

In this study we present results for waves with horizontal wavelengths (λ_x) of 30, 100, 300, and 1000 km. For each value of λ_x, 100 waves were simulated having horizontal phase speeds ranging from a minimum of 10 m s^{-1} to a maximum of 300 m s^{-1}. In all cases the simulations were performed for a nonisothermal atmosphere.

In order to help interpret the airglow temperature results we first discuss the vertical wavelength. Figure 3 shows the vertical wavelength (λ_z) plotted as a function of horizontal phase speed for each of the four values of λ_x. These values of λ_z were calculated using the isothermal dispersion equation of *Hickey and Cole* [1987] that includes the effects of dissipation and the Coriolis force, with the mean state parameters appropriate for 95 km altitude. Vertical wavelengths

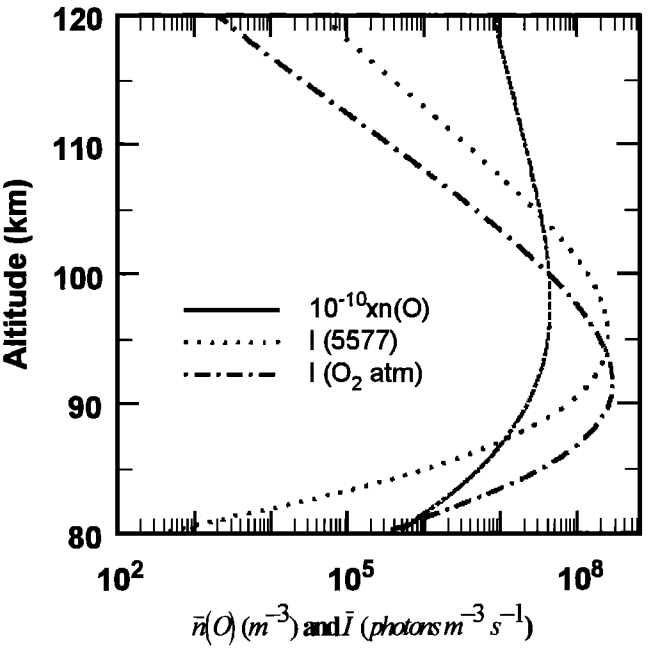

Figure 2. O profile (solid curve) derived from the MSIS-90 model and the resulting O I 5577 and O_2 atmospheric airglow volume emission rate profiles (dotted and dash-dot curves, respectively). See text for details.

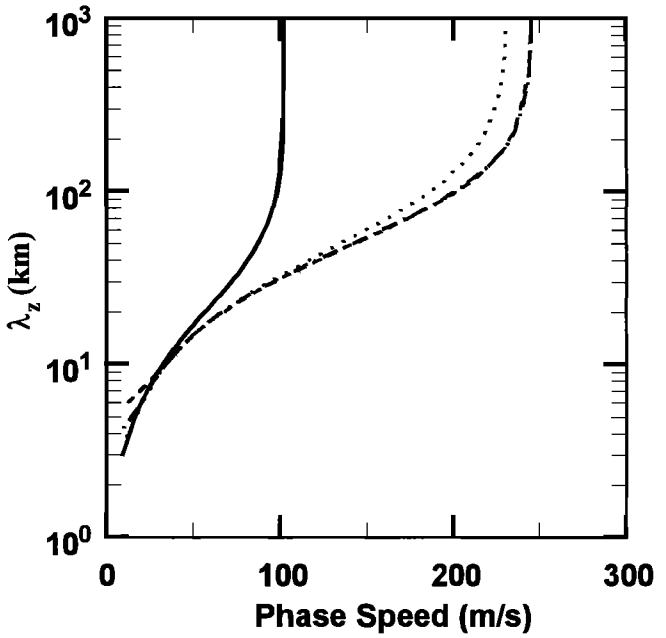

Figure 3. Vertical wavelength versus horizontal phase speed calculated using the dispersion equation of *Hickey and Cole* [1988] for horizontal wavelengths of 30 km (solid curve), 100 km (dotted curve), 300 km (dashed-dotted curve), and 1000 km (dashed curve).

corresponding to the internal acoustic wave branch are not shown. Large values of λ_z are associated with the fast internal gravity waves (with short periods), and λ_z decreases with decreasing phase speed (increasing period). This decrease of λ_z with decreasing phase speed leads to a reduction in the column-integrated airglow volume emission rate (brightness) perturbation for the slower waves due to the effects of destructive interference, which are strong whenever λ_z is less than or comparable to the emission layer thickness [*Hines and Tarasick*, 1987; *Schubert and Walterscheid*, 1988; *Swenson and Gardner*, 1998] The results displayed in Figure 3 show that values of λ_z equal to about 15 km (the nominal emission layer thickness) are achieved for waves with phase speeds of about 50 m s^{-1}.

In the following subsections we compare $\langle T_I' \rangle$ to each of $\langle T_I' \rangle$, $T'_{at-peak}$, and T'_{avg} by plotting the relevant ratios as a function of horizontal phase speed for each of the four values of horizontal wavelength. We are interested in determining at what phase speeds (and vertical wavelengths) these ratios first begin to depart from unity, and then at what phase speeds these ratios begin to differ considerably from unity. For the present comparisons we make the reasonable assumption that airglow temperatures can be determined to within about 30% using present measurement techniques, and accordingly we define a ratio to be considerably different from unity if it has a value of less than about 0 7 or greater than about 1.3.

4.1. Reflection and Evanescent Effects in $\langle T_I' \rangle / \langle T_I' \rangle$

The very largest values of λ_z shown in Figure 3 correspond to evanescent waves, and occur for phase speeds greater than about 100 m s^{-1} (for λ_x= 30 km) and greater than about 230 - 245 m s^{-1} (for all other λ_x). Evanescent waves (and acoustic waves) are not germane to this paper, although interesting interference effects due to wave reflection in a nonisothermal atmosphere associated with waves of large λ_z or evanescent wave behavior were noticed in most of our results for some of the faster waves.

Figure 4 shows the ratio $\langle T_I' \rangle / \langle T_I' \rangle$ plotted as a function of phase speed for the O I 5577 emission and for λ_x= 30 km. In this figure the evanescent wave regime is bounded by phase speeds of about 80 m s^{-1} and 120 m s^{-1}, which correspond to periods of about 6.3 min (the approximate Brunt-Vaisala period at 95 km altitude) and 4.2 min (the approximate acoustic cutoff period), respectively. Therefore, for this particular value of λ_x internal gravity waves exist for phase speeds less than about 80 m s^{-1}, while acoustic waves exist for phase speeds greater than about 120 m s^{-1}. We note the near unity and smooth behavior of the ratio $\langle T_I' \rangle / \langle T_I' \rangle$ in the acoustic wave regime for phase speeds greater than about 125 m s^{-1} Associated with the evanescent waves are interference effects which manifest themselves as dramatic variations in $\langle T_I' \rangle / \langle T_I' \rangle$. Clearly, these evanescent-related interference effects would cause large errors in the inferred value of T'. However, the precise nature of these effects are extremely sensitive to the particular details of the atmospheric temperature (and O) profile and so are not really observationally relevant. Therefore, for the remainder of this paper we present results for internal gravity waves only and truncate these results just beyond the start of the evanescent regions.

4.2. Volume Emission Rate Weighted T' as a Measure of the Mean Volume Emission Rate Weighted T' : $\langle T_I' \rangle / \langle T_I' \rangle$

Figure 5 shows $\langle T_I' \rangle / \langle T_I' \rangle$ plotted as a function of phase speed for the four waves (λ = 30, 100, 300, and 1000 km) derived from the full-wave model. For gravity waves with phase speeds greater than about 80 m s^{-1} this ratio is

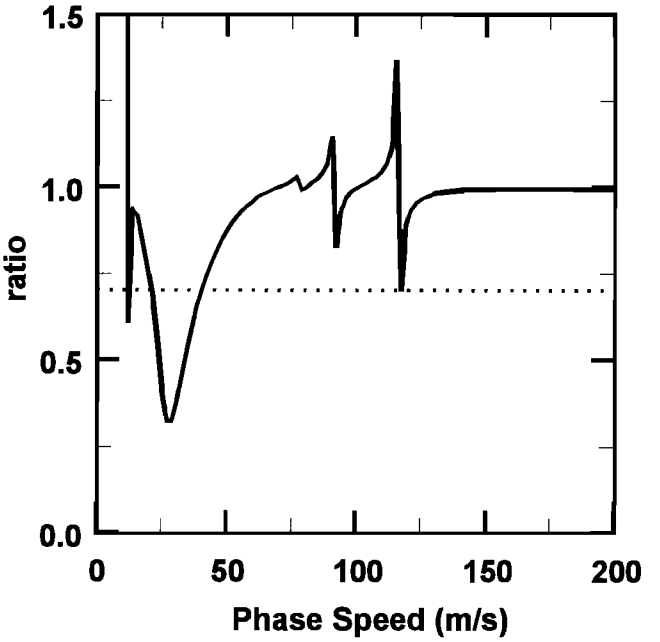

Figure 4. Magnitude of $\langle T_I' \rangle / \langle T_I' \rangle_{ISO}$ versus horizontal phase speed for waves with a horizontal wavelength of 30 km and for the O I 5577 emission. A line of a constant ratio equal to 0.7 is shown for reference.

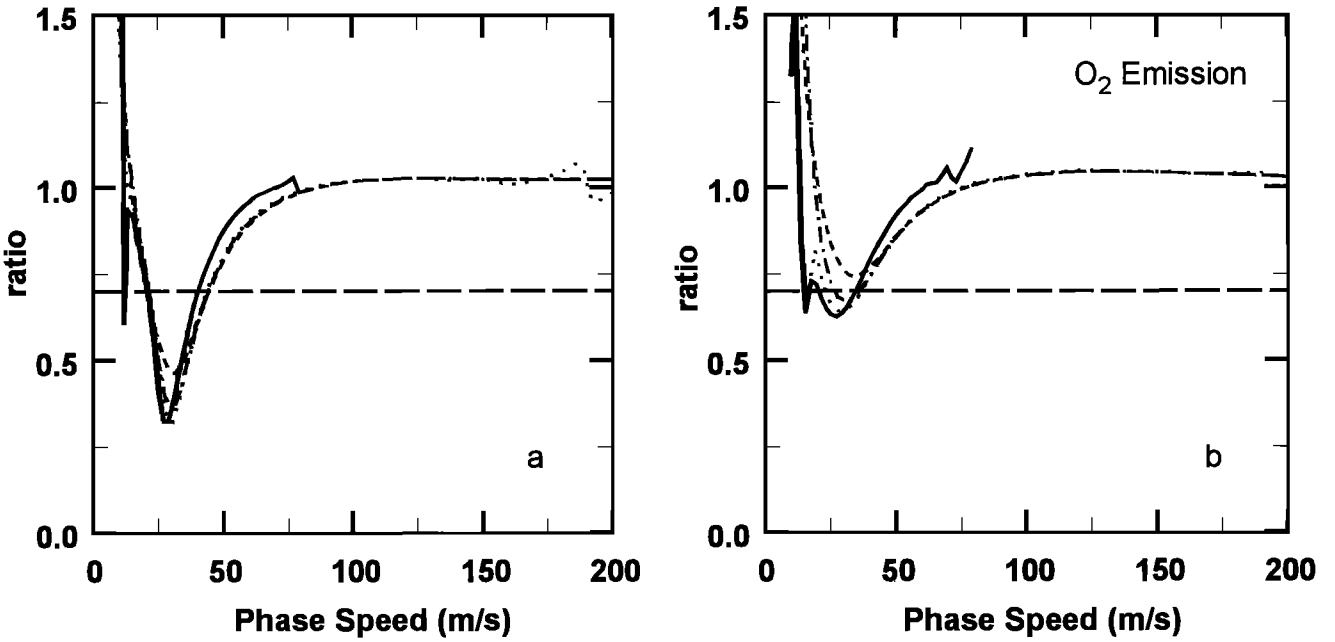

Figure 5. Magnitude of $\langle T_I' \rangle / \langle T_I' \rangle_{ISO}$ versus horizontal phase speed for waves with horizontal wavelengths of 30 km (solid curve), 100 km (dotted curve), 300 km (dashed-dotted curve), and 1000 km (dashed curve) for (a) the O I 5577 emission and (b) the O_2 atmospheric emission. A line of a constant ratio equal to 0.7 is shown for reference.

approximately unity (the slight departure from unity in this region is due to the effects of partial reflections, as previously discussed, while the departure from unity for the fastest waves is due to the evanescent behavior of these waves). For slower phase speeds the ratio decreases to values smaller than unity, reaching a local minimum of about 0.3 for phase speeds of about 32 m s^{-1}. For the O I 5577 emission the ratio first achieves a value of about 0.95 for phase speeds near 68 m s^{-1} (corresponding to $\lambda_z \sim 21$ km), and falls to a value of about 0.7 for phase speeds of about 45 m s^{-1} ($\lambda_z \sim 13$ km). For the O_2 atmospheric emission the ratio falls to values of 0.95 and 0.7 at the smaller phase speeds of about 64 and 34 m s^{-1}, respectively. Given that the ratio departs significantly from unity for waves having vertical wavelengths of about 13 km, which is comparable to the airglow emission layer thickness of both emissions (~15 km), these results show that nonisothermal effects are important for some of the slower, observable gravity waves.

4.3. Volume Emission Rate Weighted T' as a Measure of $T'_{at\text{-}peak}$: $\langle T_I' \rangle / T'_{at\text{-}peak}$

The value of $\langle T_I' \rangle / T'_{at-peak}$ is shown as a function of wave phase speed in Figure 6 for the four values of horizontal wavelength. It is clear that $\langle T_I' \rangle / T'_{at-peak}$ differs significantly from unity at most phase speeds for the internal gravity waves. $\langle T_I' \rangle / T'_{at-peak}$ falls to a value of 0.7 for phase speeds of about 90 m s^{-1} ($\lambda_z \sim 28$ km, for the O I 5577 emission) and 84 m s^{-1} ($\lambda_z \sim 25$ km, for the O_2 atmospheric emission). This implies that the temperature perturbation at the peak of the emission layer can be approximated by the volume emission rate weighted temperature perturbation only for waves of large vertical wavelength ($\lambda_z > 28$ km), so that one cannot a priori assign a temperature amplitude at a fixed altitude to temperature perturbations inferred from airglow observations. The differences that occur for $\lambda_z < 28$ km are primarily due to the cancellation effects of destructive interference, which is important for the shorter vertical wavelength waves.

4.4. Volume Emission Rate Weighted T' as a Measure of T'_{avg} : $\langle T_I' \rangle / T'_{avg}$

Figure 7 shows $\langle T_I' \rangle / T'_{avg}$ plotted as a function of horizontal phase speed for the four values of horizontal wavelength. This ratio remains approximately constant with a value close to unity for short and intermediate wave periods for the four values of horizontal wavelength. The ratio $\langle T_I' \rangle / T'_{avg}$ begins to depart from unity at a phase speed of about 64 m s^{-1} ($\lambda_z \sim 18$ km) and 54 m s^{-1} ($\lambda_z \sim 15$ km) for the O I 5577 and O_2 emissions, respectively. The ratio departs considerably from unity for phase speeds of about 50 m s^{-1} ($\lambda_z \sim 14$ km) and 45 m s^{-1} ($\lambda_z \sim 13$ km) for the O I 5577 and O_2 emissions, respectively. These values of λ_z are also greater than the thickness of the emission layer, implying that only for fast waves (45 to 50 m s^{-1}) with large vertical wavelengths ($\lambda_z \geq 14$ km) does the volume emission rate weighted temperature approximate the temperature perturbation averaged over the vertical extent of the emission region.

5. Discussion

In this study we have simulated fluctuations in the O_2 atmospheric and O I 5577 airglow intensities and then calculated a volume emission rate weighted temperature using (2). However, the temperature inferred from O I 5577 airglow observations by a high-resolution Fabry-Pérot interferometer (which measures the width of a single emission line) is necessarily the Doppler temperature. Results presented by *Makhlouf et al.* [1995] indicate that in general the volume emission rate weighted temperature perturbation differs from

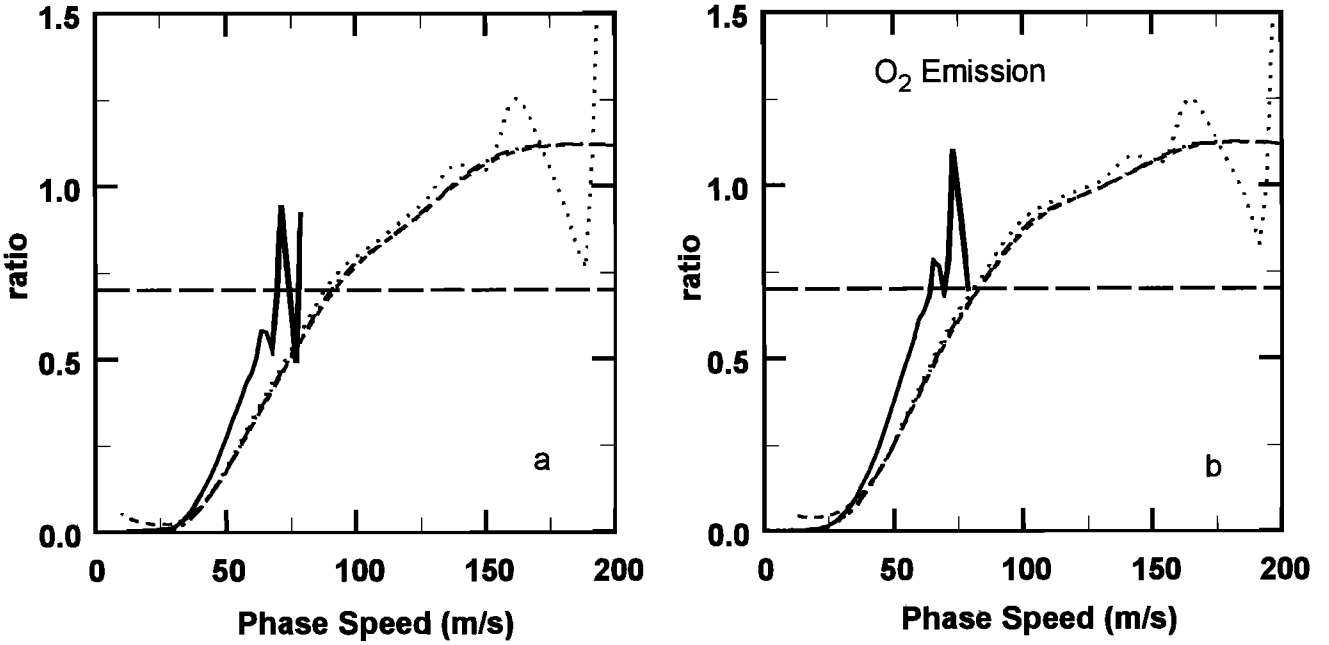

Figure 6. Similar to Figure 5 except for the ratio $\langle T_I' \rangle / T_{peak}'$.

the Doppler temperature perturbation by no more than about 20% (see their Figures 6 and 7) at all wave periods in a fairly systematic way By comparison differences between the emission rate weighted temperature perturbation and the rotational temperature perturbation are smaller. The interested reader is referred to *Makhlouf et al* [1995] for more information. We believe that our use of the volume emission rate weighted temperature perturbation will not affect the conclusions of our paper. The similarity in results obtained for the O_2 atmospheric and O I 5577 emissions tends to support that claim In a study similar to ours, *Swenson and Gardner* [1998] have successfully adopted this approach by assuming that the volume emission rate weighted temperature is equal to the rotational OH temperature. This assumption did not significantly affect the conclusions of their paper, and it is reasonable to assume that this assumption does not significantly affect our conclusions.

We studied the effects of dissipation on our results by re-running the models for "almost" adiabatic wave motions (this involved reducing the eddy diffusion coefficients to a small fraction of their nominal values). We found that while this affected the results for the slow waves (as expected), it did not affect the precise values of phase speed where the various ratios began to depart from unity. This is not really surprising,

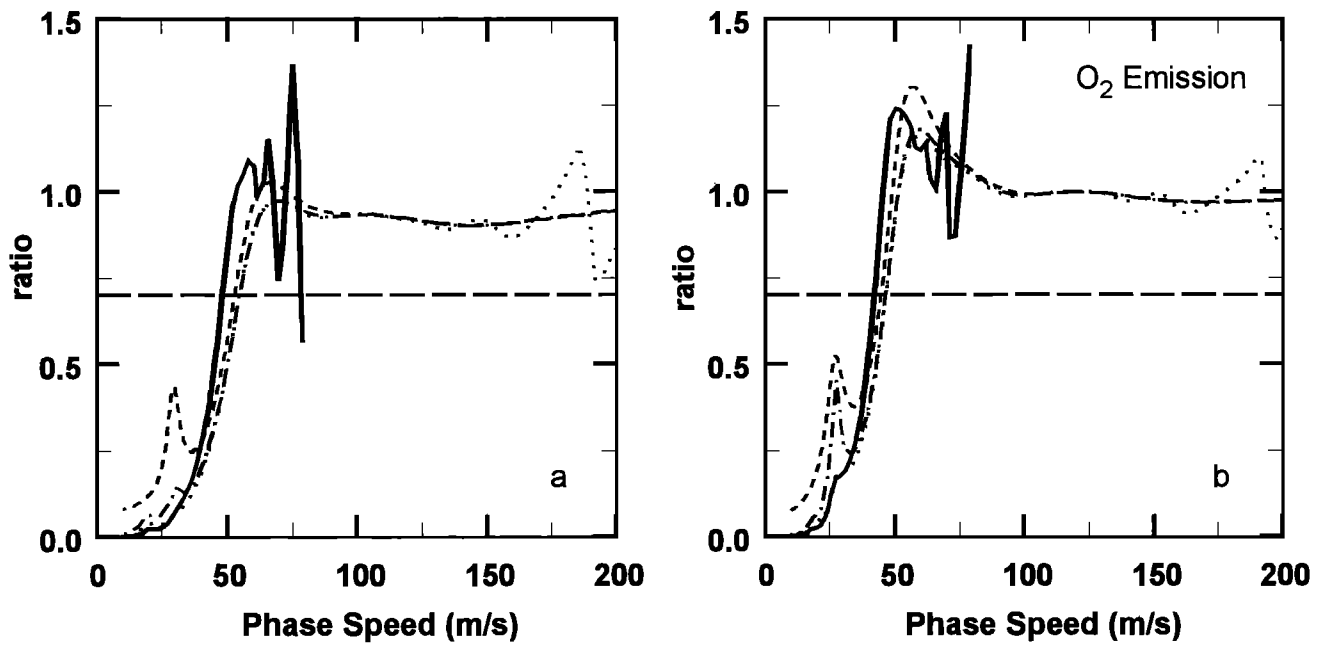

Figure 7. Similar to Figure 5 except for the ratio $\langle T_I' \rangle / T_{avg}'$.

because the departure from unity of the three ratios $\langle T_I' \rangle / \langle T_I' \rangle$, $\langle T_I' \rangle / T'_{at-peak}$, and $\langle T_I' \rangle / T'_{avg}$ occurred at phase speeds of about 68, 120, and 64 m s^{-1}, respectively. Waves with phase speeds as large as this (and with correspondingly large values of λ_z) are not significantly dissipated in this region of the atmosphere for our nominal values of eddy diffusion coefficients.

For slow waves with short vertical wavelengths the effects of destructive interference become severe and cause $\langle T_I' \rangle$ to be significantly different from either $T'_{at-peak}$ or T'_{avg} (see Figures 6 and 7, respectively). By further comparing these short vertical wavelength results shown in Figures 6 and 7 with those shown in Figure 5, we conclude that interference effects dominate over non-isothermal effects for waves with short vertical wavelengths.

We have chosen to examine the amplitudes of the perturbation quantities while recognizing that the phases of the perturbations are also important. We expect that the differences between different phase quantities become important at the same periods that the differences between the different amplitude quantities become important, as expected. The determination of wave energetics depends very sensitively on the wave amplitude and also on the relative phase difference between fluctuating quantities (one such example is the sensible heat flux, which depends on the amplitudes of w' and T' and their phase correlation).

Because $\langle T_I' \rangle$ depends on mean temperature gradients through the nonthermal terms on the right side of equation (2), the precise height of the mesopause region with respect to the height of the airglow emission layer will also determine the importance of the importance of the nonthermal contribution to $\langle T_I' \rangle$. Therefore, the importance of these nonthermal terms will depend on latitude, season (the mesopause is higher in summer than winter), and also on the particular nightglow emission of interest The nonthermal terms will be more important if the emission layer is in the region of steep temperature increase above the mesopause, implying that they will be more important for the $O(^1S)$ and O_2 atmospheric emissions (that peak near 97 km and 92 km, respectively) than for the OH emission (that peaks near 87 km). For our simulations the O I 5577 volume emission rate peak occurred 2 km below the mesopause. Had we performed our simulations for local winter conditions (and for a lower mesopause) we may have found the effects of mean temperature gradients to become important at shorter vertical wavelengths and for slower waves than we have found here. *Swenson and Gardner* [1998] studied wave-driven fluctuations of the OH Meinel emission and concluded from their simulations that the rotational temperature is very sensitive to the shape of the background temperature profile and mean temperature gradients, especially for waves with λ_z < 15 km. However, for waves with $\lambda_z \geq$ 15-18 km they found that the temperature profile did not influence the airglow response to waves. By comparison, we find here that mean temperature gradients are important at the higher altitudes of the O I 5577 emission for waves with λ_z < 25 km.

The effects discussed in the last paragraph will also depend on other mean-state parameters, such as the major gas density (which affects quenching) and the atomic oxygen (O) density (which affects airglow production). Of these, O densities are highly variable, with a strong dependence on local time as well as on season and latitude. Obviously our conclusions will be affected to some degree on the assumed O profile (provided by the MSIS model) and its displacement relative to the mesopause height. However, such considerations lie beyond the scope of this short paper.

We note that whenever nonisothermal effects make a non-negligible contribution to the airglow emission perturbations (through equation (2)) they would also be expected to be important in the gravity wave dynamics themselves. Under these circumstances, full-wave modeling is usually required to correctly include terms involving mean temperature gradients in the wave equations, and this is another feature of our study not included in the analysis of *Swenson and Gardner* [1998]. However, mean temperature gradients are more important for the very fast waves having large vertical wavelengths (λ_z > 28-50 km), and so should not significantly affect the conclusions of *Swenson and Gardner* [1998].

This study has shown that for some of the slower but still observable gravity waves numerical modeling is required to determine gravity wave amplitudes given the observed values of $\langle T_I' \rangle$. We have also shown that the volume emission rate perturbation must generally be calculated in any case for most gravity waves with vertical wavelengths λ_z < 13-25 km (the nonthermal terms in (2)). Thus it is our belief that under such circumstances it is easier to determine the wave amplitude using only the observed brightness fluctuations and a realistic model. In the case of the O I 5577 emission there is an additional and important advantage to such an approach. Temperatures inferred from the O I 5577 emission usually require very long integration times (~ 1 hour) in order to achieve the desired accuracy, so that such measurements can provide information only for waves with periods of at least ~3 hours (e.g., Schubert et al., submitted manuscript, 1998). By comparison brightness fluctuations measured in the O I 5577 nightglow emission have been successfully used to measure gravity waves with periods as short as several minutes [e.g., *Taylor and Garcia*, 1995; *Taylor et al*,. 1997], and these measured brightness fluctuations were subsequently modeled by *Hickey et al.* [1997, 1998] in order to determine wave amplitudes. Thus, for the O I 5577 emission, amplitude information can only be obtained for gravity waves with periods of less than a few hours by combining brightness measurements with modeling. Therefore the modeling has dramatically improved the usefulness of the O I 5577 emission as a diagnostic of gravity waves in the mesopause region.

Although we have only discussed the interpretation of gravity waves in nightglow emissions our results may also be applicable to the interpretation of tidal variations in the nightglow. In particular our results might apply to the interpretation of diurnal temperature amplitudes inferred from nightglow emissions because the vertical wavelength of the diurnal tide can be comparable to the vertical scales at which the nonthermal effects become important Our results would not, in general, apply to the semi-diurnal tide because its vertical wavelength generally exceeds 50 km.

6. Conclusion

Our results show that $\langle T_I' \rangle$ can provide a measure of the temperature perturbation at the altitude of the emission peak, $T'_{at-peak}$, only for large vertical wavelengths satisfying λ_z > 28-50 km. For shorter vertical wavelengths the effects of destructive interference become important and cause $\langle T_I' \rangle$ to be significantly different from $T'_{at-peak}$. Additionally, $\langle T_I' \rangle$

can provide a measure of the mean temperature perturbation averaged over the vertical extent of the emission layer, T'_{avg}, for vertical wavelengths satisfying $\lambda_z > 16$-20 km. Our results also show that the mean volume emission rate weighted temperature perturbation, $\langle T'_I \rangle$, is only a good approximation to the full volume emission rate weighted temperature perturbation for a non-isothermal atmosphere, $\langle T'_I \rangle$, for vertical wavelengths $\lambda_z > 13$-25 km. Because the thickness of emission layers in the mesopause region is typically about 10 km, our results imply that for many observable waves $\langle T'_I \rangle$ will not approximate $\langle T'_I \rangle$, $T'_{at-peak}$, or T'_{avg}. Therefore, while both $T'_{at-peak}$ and T'_{avg} are essentially provided by $\langle T'_I \rangle$ for the fast waves with large vertical wavelengths, for some observable but slower gravity waves in the airglow the actual temperature perturbation can only be derived from measured values of $\langle T'_I \rangle$ using chemical-dynamical models. In general, the complete nonisothermal value of $\langle T'_I \rangle$ needs to be modeled, because its nonisothermal equivalent, $\langle T'_I \rangle$, departs from $\langle T'_I \rangle$ in the same regime where the modeling is in any case required.

Numerical modeling similar to that performed here could be used to determine gravity wave amplitudes given the observed values of $\langle T'_I \rangle$. However, because we have shown that the volume emission rate perturbation must generally be calculated in any case for most gravity waves with vertical wavelengths $\lambda_z < 13$-25 km (the nonthermal terms in (2)), we believe that under such circumstances given the observed brightness fluctuations alone, wave amplitude would be easier determined using the approach of *Hickey et al.* [1997, 1998]. *Swenson and Gardner* [1998] have forwarded a similar conjecture. Also, because these short vertical wavelength waves are apt to break or dissipate in the mesopause region determining their amplitudes more accurately from airglow observations may provide additional useful information concerning the contribution by gravity waves to the energetics of this region.

Acknowledgments. During the course of this research MPH was supported by NSF grant ATM-9612819 and NASA grant NAG5-4762, and RLW was supported by NASA grant NAG5-4528. The authors thank the referees for their useful and substantive comments.

Janet G. Luhmann thanks Jeng-Hwa Yee and another referee for their assistance in evaluating this paper.

References

Hecht, J. H., and R. L. Walterscheid, Observations of the OH Meinel (6,2) and O_2 atmospheric (0,1) nightglow emissions from Maui during the ALOHA-90 campaign, *Geophys. Res. Lett., 18*, 1341, 1991.

Hedin, A. E., Extension of the MSIS thermosphere model into the middle and lower atmosphere, *J. Geophys. Res., 96*, 1159, 1991.

Hickey, M. P., Effects of eddy viscosity and thermal conduction and Coriolis force in the dynamics of gravity wave driven fluctuations in the OH nightglow, *J. Geophys. Res., 93*, 4077, 1988.

Hickey, M. P., and K. D. Cole, A quartic dispersion equation for internal gravity waves in the thermosphere, *J. Atmos. Terr. Phys., 49*, 889, 1987.

Hickey, M. P., G. Schubert, and R. L. Walterscheid, Gravity wave-driven fluctuations in the O_2 atmospheric (0-1) nightglow from an extended, dissipative emission region, *J. Geophys. Res., 98*, 13,717, 1993.

Hickey, M. P., R. L. Walterscheid, M. J. Taylor, W. Ward, G. Schubert, Q. Zhou, F. Garcia, M. C. Kelley, and G. G. Shepherd, Numerical simulations of gravity waves imaged over Arecibo during the 10-day January 1993 campaign, *J. Geophys. Res., 102*, 11,475, 1997.

Hickey, M. P., M. J. Taylor, C. S. Gardner, and C. R. Gibbons, Full-wave modeling of small-scale gravity waves using Airborne Lidar and Observations of the Hawaiian Airglow (ALOHA-93) O(^{1}S) images and coincident Na wind/temperature lidar measurements, *J. Geophys. Res., 103*, 6439, 1998.

Hines, C. O., and D. W. Tarasick, On the detection and utilization of gravity waves in airglow studies, *Planet. Space Sci., 35*, 851, 1987.

Hines, C. O., and D. W. Tarasick, Airglow response to vertically standing gravity waves, *Geophys. Res. Lett., 21*, 2729, 1994.

Makhlouf, U., R. H. Picard, and J. R. Winick, Photochemical-dynamical modeling of the measured response of airglow to gravity waves, I, Basic model, *J. Geophys. Res., 100*, 11,289, 1995.

Makhlouf, U. B., R. H. Picard, J. R. Winick, and T. F. Tuan, A model for the response of the atomic oxygen 557.7 nm and the OH Meinel airglow to atmospheric gravity waves in a realistic atmosphere, *J. Geophys. Res., 103*, 6261, 1998.

Schubert, G., and R. L. Walterscheid, Wave-driven fluctuations in OH nightglow from an extended source region, *J. Geophys. Res., 93*, 9903, 1988.

Schubert, G., R. L. Walterscheid, and M. P. Hickey, Gravity wave-driven fluctuations in OH nightglow from an extended, dissipative emission region, *J. Geophys. Res., 96*, 13,869, 1991.

Swenson, G. R., and C. S. Gardner, Analytic models for the responses of the mesospheric OH* and Na layers to atmospheric gravity waves, *J. Geophys. Res., 103*, 6271, 1998.

Taylor, M. J., and F. J Garcia, A two-dimensional spectral analysis of short period gravity waves imaged in the OI(557.7 nm) and near-infrared OH nightglow emissions over Arecibo, Puerto Rico, *Geophys. Res. Lett., 22*, 2473, 1995.

Taylor, M. J., W. R. Pendleton Jr., S. Clark, H. Takahashi, D. Gobii, and R. A. Goldberg, Image measurements of short period gravity waves at equatorial latitudes, *J. Geophys. Res., 102*, 26,283, 1997.

M. P. Hickey, Department of Physics and Astronomy, 308 Kinard Laboratory, Clemson University, Clemson, SC 29634-1911. (hickey@hubcap.clemson.edu.)

R. L. Walterscheid, Space and Environment Technology Center, The Aerospace Corporation, Los Angeles, CA 90009. (richard.walterscheid@aero.org.)

(Received June 25, 1998; revised October 13, 1998; accepted December 11, 1998.)